Blade–wake interactions in cross-flow turbines

Esteban Ferrer

Richard H.J. Willden

This paper presents analytical bounds for blade–wake interaction phenomenona occurring in rotating cross-flow turbines for wind and tidal energy generation (e.g. H-rotors, Darrieus or vertical axis). Limiting cases are derived for one bladed turbines and extended to the more common three bladed configuration. Additionally, we present a classification of the blade–wake type of interactions in terms of limiting tip speed ratios.

These bounds are validated using a high order h/p Discontinuous Galerkin solver with sliding meshes. This computational method enables highly accurate flow solutions and shows that the analytical bounds correspond to limiting blade–wake interactions in fully resolved flow simulations.

1. Introduction

Rotating airfoils on a fluid present a challenging problem since fluid–structure interactions are likely to occur. Examples where airfoil rotation may lead to fluid–structure interactions can be found in turbomachinery applications, helicopter aerodynamics, insect flight aerodynamics, unmanned air vehicles and flows through renewable energy devices such as wind and tidal turbines.

The effect of vortices interacting with blades and airfoils have been summarised in the past [26,6]. These effects vary from mild vibrations to unsteady loading that may result in structural fatigue and potential failure. In addition, vortex interactions often result in uncontrolled sound generation. In summary, blade vortex interactions result in non-linear processes that are difficult to control and whose effects are generally damaging in terms of aerodynamics, structural integrity and acoustics.

Prediction of the conditions that lead to such interactions are therefore of capital importance for engineering applications since they define the design envelope and influence the structural integrity of the device. Furthermore, these interactions restrict the use of simplified analytical tools or semi-empirical correlations.

Cross-flow wind and tidal turbines for power generation, also known as H-rotors, Darrieus or vertical axis turbines, present interesting interactions and complex flow phenomena. These type of turbines consist of foil shaped blades that generate lift forces so as to rotate a shaft to which the blades are connected. Therefore azimuthal changes in blade aerodynamics (or hydrodynamics if tidal devices are considered) are common, resulting in complex flow phenomena such as stalled flows, vortex shedding and blade–vortex interactions. The interested reader is referred to [18,8,33,21] for cross-flow turbines in the context of wind power generation and to [23] for its use in urban environments. Tidal turbines have become increasingly popular and their particularities can be found in [34,15,7,1].

Various engineering techniques have been developed to model flows through cross-flow turbines, but these may prove inadequate in capturing some complex flow phenomena (see [18] for a review). In particular, blade–vortex interactions are often neglected in simplified analysis codes (e.g. actuator disc or Blade Element Momentum) and hence the limits for which these solvers are accurate remain unclear. For example, popular methods for turbine applications, that can benefit from our analysis, are *lifting line* or *vortex models* methods, e.g. [18,30]. These rely on pre-existing lift and drag data to model the blade aerodynamics and allow for free development of wake structures and their evolution. However, if blade–vortex interactions occur, then *vortex models* are unable to naturally account for modifications of the lift and drag data due to the vortex impingement on the blades. Without modifying the aerodynamic coefficients, these models are unlikely to predict accurately the turbine aerodynamics. Our analysis can predetermine the range of usability of such models or even determine if corrections are needed in the lift and drag input data.

Previous works have studied wake and vortex interaction effects for particular geometries using complex numerical methods (e.g. [29,28]) but have not attempted to derive generalised analytical estimates to bound blade–wake interactions.

Our work analyses the physics involved in cross-flow turbines to derive bounds on blade–wake interactions in terms of geometrical factors (i.e. tip speed ratio). To the authors' knowledge, these analytical estimates are a first attempt to bound the various types of blade–wake interactions that may be used in the future to correct simplified models of blade element momentum type. The analytical bounds included in this paper may provide limiting conditions for analytical or algebraic models (e.g. [24,32,35,31] for cross-flow wind turbines or [34,15,7] in the tidal energy context) and also improve the understanding on the behaviour of turbine's starting conditions (e.g. [27,14]).

To validate the analysis, we present fully resolved numerical simulations of cross-flow turbines and compare the derived analytical bounds to numerical results for one and three bladed turbines. Numerous studies have computed vertical axis turbines using low order methods (e.g. [20,16,25,3,17,2,22]) but to the authors' knowledge there has not been any previous attempts to compute rotating turbines using a high order solver with sliding meshes [13,10]. The solver accuracy does not degrade when the mesh is dynamically moved and hence is well suited for the study of fluid–structure interaction phenomena [13].

The main contributions of our work can be summarised in the following bullet points:

- We present novel analytical bounds for blade–wake interaction phenomena occurring in rotating cross-flow turbines.
- We characterise the blade–wake types of interactions for one and three bladed turbines.
- We validate these analytical bounds and associated flow regimes using a high order Discontinuous Galerkin solver with sliding meshes.
- We provide novel result for rotating airfoils that may be used in the future for numerical validations.

The paper is organised as follows. First, we introduce the analytical bounds for one and three bladed turbines. Second, we compare these estimates with numerical simulations to validate our analytical bounds.

2. Analytical estimates

We first introduce the required notation and main parameters that describe cross-flow turbines, to subsequently detail the analysis of blade–wake interactions.

2.1. Preliminaries and notation

Fig. 1 shows a sketch of a typical straight bladed cross-flow turbine, where the essential parameters to characterise its geometry and operational regimes are included. The figure introduces the azimuthal angle θ (i.e. $\theta = 0^\circ$ corresponds to 12 o'clock), the free stream velocity $\mathbf{U}$ with magnitude $|\mathbf{U}| = U$, the rotational velocity $\mathbf{U_{rot}}$ with magnitude $|\mathbf{U_{rot}}| = \omega R$, where R is the turbine radius and ω the rotational speed, the effective velocity $\mathbf{U_{eff}} = \mathbf{U} + \mathbf{U_{rot}}$ and the resulting geometric angle of attack (AOA). In addition, Fig. 1 defines the Lift (L) and Drag (D) force components and their associated polar projections: Tangential (T) and Normal (N) forces. One may characterise the turbine by the tip speed ratio $\lambda = \omega R/U$, and the solidity $\sigma = Nc/R$, with N the number of blades, and c the foil chord. Lastly, the blade geometric velocity and the geometric angle of attack may be defined as: $U_{eff} = U\sqrt{1 + 2\lambda\cos\theta + \lambda^2}$ and $AOA = tan^{-1}(\frac{\sin\theta}{\lambda + \cos\theta})$.

2.2. Blade–wake interactions for rotating one bladed turbines

To analyse blade–vortex or blade–wake interactions, we need to consider and compare two physical processes: firstly, the vortex or wake generation at the upstream blade passage and its convection; secondly, the blade rotation. It is the relative times of wake convection to blade rotation that gives rise to different types of interactions. Fig. 2 illustrates the three types of interactions expected, when varying the blade rotational speed with respect to the wake convection speed, in terms of the tip speed ratio λ and various limiting cases, which are subsequently defined.

In this work, we intentionally avoid using the term "blade–vortex" interaction but favour instead "blade–wake" since the latter does not imply any particular shape or condition of the flow structures involved (such as vorticity or circulation) and is therefore more general.

A blade travelling through the upstream passage generates a wake (Fig. 2a) that is convected downstream with speed $U_{axial} = \beta U$, where U_{axial} is the mean streamwise velocity component within the turbine and β is the axial induction factor related to the front half of the turbine. This induction factor defines the deceleration of the flow when passing through the front of the turbine and relates to the flow distortion caused by the blade passage. Note that in general, the induction factor has values below unity, $0 < \beta \leq 1$, since $U_{axial} \ll U$ (i.e. flow deceleration). For a one bladed turbine rotating at a low speed, it may

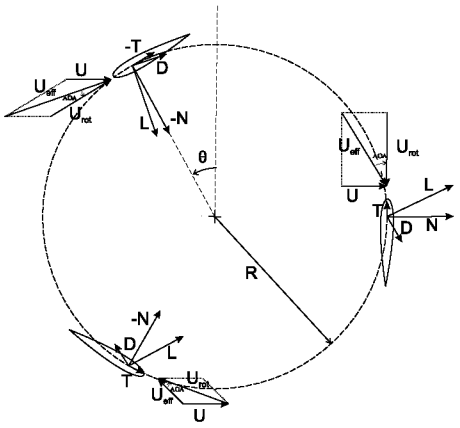

Fig. 1. Schematic of the three bladed cross-flow turbine. Free stream velocity from left to right and turbine rotating clockwise.

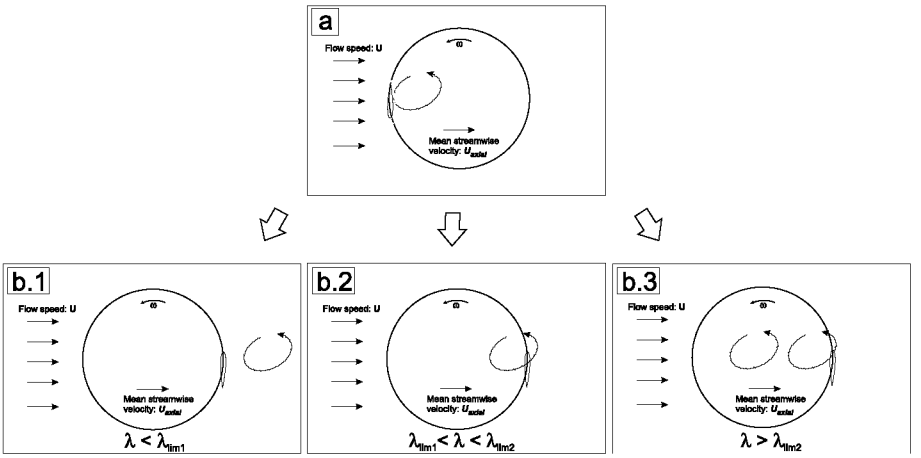

Fig. 2. Schematic of the three limiting conditions for blade–wake interactions: (a) initial wake or vortex shedding, (b.1) no blade–wake interactions, (b.2) upstream shed wake interacts with the blade at its next rear passage and (b.3) two upstream shed wakes interact with the blade at its rear passage.

be approximated to unity $\beta \approx 1$ (i.e. limited flow distortion). The interested reader is referred to [18] and references therein for theoretical approximations for the induction factor (e.g. $\beta = 1/(1 + Cdd/4)$ if a simple streamtube technique is used, with Cdd the rotor drag coefficient).

Let us now quantify the wake convection and blade rotation times. Considering the speed of wake convection ($U_{axial} = \beta U$) and the diameter of the turbine $D = 2R$, the time for the wake (or vortex) to reach the downstream section can be estimated as $t_{wake} \approx 2R/\beta U$. Regarding the blade rotation, the time for the blade to transition, from $\theta = 90^\circ$ to $\theta = 270^\circ$ is $t_{foil} = R\pi/(R\omega)$.

When comparing these times it becomes clear that for $t_{wake} < t_{foil}$, the wake shed on the upstream passage is convected aft of the turbine before the blade completes its downstream pass and there is no blade–wake interaction (e.g. Fig. 2b.1). However, if the wake convection is slower compared to the blade rotation (i.e. $t_{wake} > t_{foil}$), then the blade on the downstream section intersects the wake generated when at $\theta = 90^\circ$ and hence sees a disturbed flow that leads to a change in its aerodynamic performance (e.g. Fig. 2b.2). It can be concluded that the first limiting case for interaction to occur (Fig. 2b.2) can be calculated by setting the wake advection time to be equal to the foil time: $t_{wake}/t_{foil} \approx 1$ which can be rearranged to $t_{wake}/t_{foil} = (\frac{2R}{\beta U})/(\frac{R\pi}{R\omega}) = 2\lambda/\beta\pi \approx 1$. From the latter expression, one can isolate the limiting tip speed ratio for the first type of interaction. Doing so, it can be seen that interactions occur if $\lambda \gtrsim \lambda_{lim1} = \beta\pi/2$. Assuming that for one bladed turbines the axial induction factor is close to unity $\beta \approx 1$, we obtain the limit $\lambda_{lim1} \approx 1.6$.

For values of $\lambda < \lambda_{lim1} \approx \beta\pi/2$ one can still expect interactions but only for angles comprised between $180^\circ < \theta < 270^\circ$ (low rear quadrant). This is due to the proximity of the blade to the previously shed wake when in the lower half of its circular path. This last case can be analysed by considering an arbitrary chord of the circular path (and not the diameter) $chr = 2R\sin(\varphi/2)$ with associated arc length $arc = \varphi R$ for an arbitrary angle $0^\circ < \varphi < 180^\circ$. A new generalised limiting case for interactions for azimuthal angles within $180^\circ < \theta < 270^\circ$ can then be estimated using the relationship $t_{wake}/t_{foil} = \left(\frac{2R\sin(\varphi/2)}{\beta U}\right)/\left(\frac{\varphi R}{R\omega}\right) = 2\lambda\sin(\varphi/2)/(\beta\varphi) \approx 1$. For small enough angles φ, a Taylor series approximation of $\sin(\varphi/2) \approx \varphi/2$ leads to the tip speed ratio limit $\lambda_{lim1-chord-based} = \beta$. Finally, it can be concluded that for values of $\lambda < \lambda_{lim1-chord-based} = \beta$ no interactions at all are present. Let us note that this last expression provides an indirect way to estimate the induction factor β of a given turbine by checking the conditions (e.g. the tip speed ratio) for which the interactions are not present.

For values of the tip speed ratios between $\lambda_{lim1-chord-based} < \lambda < \lambda_{lim1}$, interactions should only occur at the bottom half of the circular path, (i.e. azimuthal angles of $180^\circ < \theta < 270^\circ$).

Following the same reasoning as for the derivation of the first limit $\lambda_{lim1} = \beta\pi/2$ (i.e. considering a wake shed at $\theta = 90^\circ$ and intersecting the blade at $\theta = 270^\circ$), a second limiting case can be found for

$\lambda > \lambda_{lim2} = 3\pi\beta/2$. The latter is obtained by considering $t_{wake} \approx 2R/\beta U$ and $t_{foil} = 3R\pi/(R\omega)$. This corresponds to the blade travelling 1.5 revolutions (from $\theta = 90^\circ$ to $\theta = 630^\circ$) and the first wake (shed at $\theta = 90^\circ$) not having been convected aft of the turbine as sketched in Fig. 2b.3. This case correspond to low tip speed ratios where the blade rotation speed is much faster than the free stream velocity. For this last case, a cumulative wake effect (i.e. two wakes have been shed) is to be expected, since the wakes being shed by the foil at $\theta = 90^\circ$ and $\theta = 450^\circ$ have an impact on the blade performance once it reaches $\theta = 630^\circ$ and then at every 360° past that angle. If we further assume an axial induction factor of one, $\beta \approx 1$, we can approximate this second limit to $\lambda_{lim2} \approx 4.7$.

The derived limits for one bladed turbines can be summarised as:

- $\lambda < \beta$: No interactions.
- $\beta < \lambda < \lambda_{lim1} = \beta\pi/2 \approx 1.6\beta$: Interactions limited to the low rear quadrant.
- $\lambda_{lim1} < \lambda < \lambda_{lim2} = 3\beta\pi/2 \approx 4.7\beta$: blade interacts with one wake near $\theta = 270^\circ$ (see Fig. 2b.2).
- $\lambda_{lim2} < \lambda$: blade interacting with two wakes or more (see Fig. 2b.3).

2.3. Blade–wake interactions for rotating three bladed turbines

The reasoning detailed in the previous section can be extended to the more interesting case of a three bladed turbine. In this case, we obtain the following estimates for the blade–wake interaction limits:

- $\lambda_{lim1} = \beta\pi/6 \approx 0.5\beta$: blade interacts with one wake. In this case, the wake shed by a front passing blade at $\theta \approx 90^\circ$ can be intercepted by another blade after rotating an angle $\triangle\theta = 60^\circ$ an hence t_{foil} is one third of the airfoil time considered in the one bladed case. To obtain this limit we have used $t_{wake} \approx 2R/\beta U$ and $t_{foil} = R\pi/(3R\omega)$.
- $\lambda_{lim2} = \beta\pi/2 \approx 1.6\beta$: blade interacting with two wakes shed upstream. In this case, the blade that has shed the wake during the front passage interacts with its own wake when reaching $\theta \approx 270^\circ$. This is similar to the one bladed case, however when three blades are present, another wake has been shed when the interaction takes place, and hence for this tip speed ratio two wakes need to be considered.
- $\lambda_{lim3} = 5\beta\pi/6 \approx 2.6\beta$: blade interacting with three wakes. For this case we have used: $t_{wake} \approx 2R/\beta U$ and $t_{foil} = 5R\pi/(3R\omega)$.

For three bladed turbines the induction factor β is expected to be smaller than unity (due to an increased solidity or blockage leading to more important flow deceleration) and hence the limiting tip speed ratios λ_{lim} (that depends on β) should be lower than for one bladed turbines. To obtain induction factors larger than unity, the flow needs to accelerate through the front passage of the turbine, which is generally not the case unless ducted turbines are considered.

2.4. Summary of blade–wake interactions

Finally, Table 1 summarises the analytical bounds for one and three bladed turbines. The table includes the limiting tip speed ratios, the type of interactions that can be encountered for each regime, together with the azimuth angles where an effect is to be seen when analysing the forces on a rotating blade.

3. Numerical validation

In this section we validate the derived analytical estimates using a high order h/p Discontinuous Galerkin (DG) solver with sliding meshes [13,10,12,11]. In this work we extend this unstructured solver to the simulation of fluid-structure interactions as encountered in cross-flow turbines. We consider a generic turbine and compare the analytical bounds derived in previous sections to the simulations. The geometries studied in this section are characterised by their radius $R = 2c$ and their solidities $\sigma = Nc/R = 1/2$ with $N = 1$ for the one bladed turbine, and $\sigma = 3/2$ with $N = 3$ for the three bladed turbine. The blade sectional normal and tangential forces are non-dimensionalised using the free stream velocity magnitude: $C_j = 2F_j/\rho cU^2$, where $j = N, T$ and ρ the fluid density.

Table 1
Summary of blade–wake interactions and its effects on blade forces.

One bladed				
Tip speed ratio limit	$\lambda < \beta$	$\beta < \lambda < \beta\pi/2$	$\beta\pi/2 < \lambda < 3\beta\pi/2$	$3\beta\pi/2 < \lambda$
Type of interaction	No inter.	Limited	One-wake	Two-wakes or more
Force effect with azimuth	–	$180^\circ < \theta < 270^\circ$	$180^\circ < \theta < 360^\circ$	Everywhere
Three bladed				
Tip speed ratio limit	$\lambda < \beta\pi/6$	$\beta\pi/6 < \lambda < \beta\pi/2$	$\beta\pi/2 < \lambda < 5\beta\pi/2$	$5\beta\pi/2 < \lambda$
Type of interaction	Limited	One-wake	Two-wakes	Three-wakes or more
Force effect with azimuth	$180^\circ < \theta < 270^\circ$	$180^\circ < \theta < 360^\circ$	Everywhere	Everywhere

Table 2
Flow conditions and turbine characteristics for 2D simulations.

Free stream velocity U [m/s]	Rotational speed ω [rad/s]	Tip speed ratio λ [–]
0.2	0.5	5
0.5	0.5	2
1.0	0.5	1

Table 2 summarises the flow conditions and turbine characteristics considered in this section. Namely, three tip speed ratios (λ) are studied by varying the free stream speed (U), while maintaining constant the rotational speed (ω).

3.1. High order numerical method

Flow solutions of the non-linear incompressible Navier-Stokes equations, are obtained from the 3D unsteady high order (*order* $\geqslant 3$) h/p Discontinuous Galerkin (DG) – Fourier solver developed by the authors [13,10,12,11]. This high order solver provides highly accurate solutions on static and moving meshes composed of mixed triangular-quadrilateral meshes and can cope with curved boundary elements. Before proceeding to the validation section, we illustrate the advantage of high order methods over low order methods by presenting solution snapshots of laminar vortex shedding (chord Reynolds number $Re = 800$) aft a NACA0012 using the developed DG solver and the finite volume code Ansys-Fluent in Fig. 3. The DG solution has been obtained using a mesh constituted of 798 tri-quad elements and a polynomial order $k = 5$ leading to a total number of degrees of freedom DOF=17448. The finite volume solution required second order discretisation in space and time and a mesh constituted of 29516 DOF (1.7 times more DOF than the DG solution). We note the low numerical diffusivity on the shed vortices for the high order DG code when compared to the lower order solution.

It is this feature of high order spectral h/p and DG methods that has led to their increased popularity in the flow simulation community. In addition, the ability to convect vortex structures with minimal numerical distortion makes this high order implementation particularly suitable to simulate blade–vortex and blade–wake interactions.

3.2. Cross-flow turbine simulations

Two distinct but complementary problems are simulated:

1. **One bladed turbine**: analysis of the influence of the wake generated through the upstream passage on the downstream blade passage: blade–wake or blade–vortex interactions. Validation of analytical bounds.
2. **One bladed and three bladed turbines**: analysis of the fluid-dynamic differences between one and three bladed turbines and validation of bounds for blade–wake interactions.

Fig. 4 shows DG results (using a polynomial order $k = 3$) for the one and three bladed turbines. All meshes are constituted of triangular-quadrilateral elements: 1794 elements for the one bladed turbine mesh depicted partially in Fig. 4a, b, and c; and 3320 elements for the three bladed turbine in

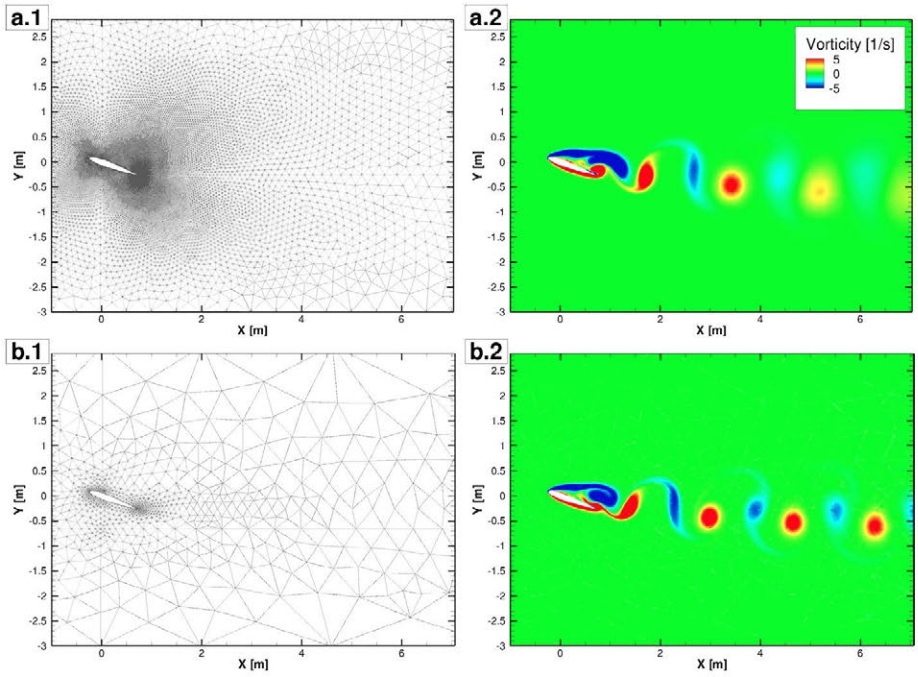

Fig. 3. Mesh and snapshots of vorticity for the vortex shedding aft a NACA0012 at $Re = 800$ and AOA$= 20°$: (a) Finite volume code (b) DG solver.

Fig. 4d. The three snapshots for the one bladed turbines, Fig. 4a, b, and c, have been selected such that the blade azimuthal angles coincide with the blade positions for the three bladed case Fig. 4d. These snapshots show that one and three bladed turbines present substantially different flow fields, which will be subsequently analysed. In addition, it can be seen that the code preserves wake structures and predicts blade–wake interactions for these complex flows.

The Reynolds numbers, based on the blade chord and the free stream velocity U (i.e. without accounting for the rotational velocity), are low $Re \approx 100$ which enables direct numerical simulation without turbulence modelling. This avoids inaccuracies and uncertainties inherited from selecting a turbulent closure model (e.g. [1,19,25,9] for turbine simulations). However, to show the validity of the simulations and the analysis for a range of Reynolds numbers, we include in the appendix a comparison of blade forces and flow fields for various Reynolds numbers. Fig. 9 in the appendix shows comparisons of blade forces for one bladed turbines and varying Reynolds numbers $Re = 100$, 1000 and 10.000 Note that for $Re = 10.000$ the flow can be considered turbulent. In addition, flow fields for various Reynolds numbers are shown in Fig. 10. Both force traces and flow fields show that blade–wake interactions have similar character for all Reynolds numbers.

Finally, let us note that the result included herein have a fundamental character since they explore novel physics of rotating airfoils. Furthermore, we provide novel results for rotating airfoils that may be used to validate new numerical tools or even design microturbines for medical applications (e.g. [5,4]). Indeed, to the authors' knowledge there is no published data for validation of unsteady aerodynamics such as the results presented in this paper (i.e. direct numerical simulations of rotating airfoils).

3.2.1. One bladed turbine

Before proceeding to the physical investigations, the necessary spatial resolution is investigated. Namely, we find the required polynomial order k for the given mesh to obtain accurate results, i.e. unchanged when increasing the spatial resolution. To this end, Fig. 5 compares the tangential and normal force traces against azimuth for a one bladed turbine using two polynomial orders $k = 2$ and 3, for two tip speed ratios $\lambda = 1$ and 2.

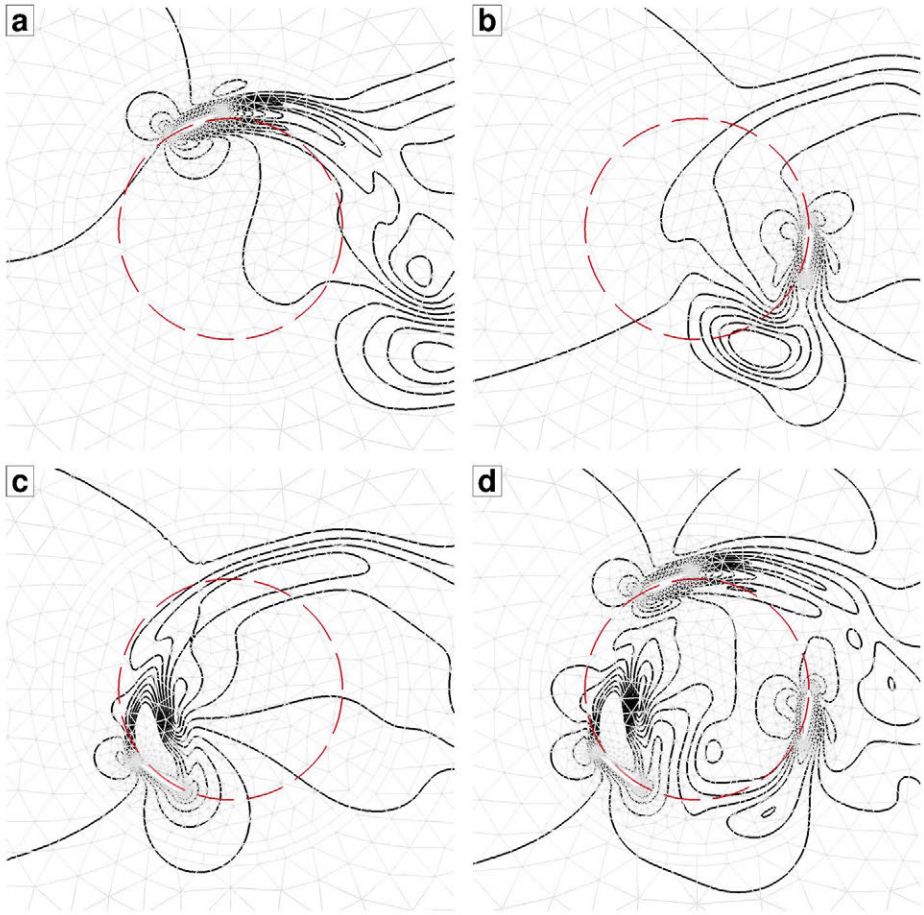

Fig. 4. DG flow field snapshots of velocity magnitude for $\lambda = 2$: (a)–(b)–(c) one bladed turbine at three azimuthal positions and (d) three bladed turbine. Red dashed line shows the circular blade path.

It can be seen that the results are unchanged when using a higher resolution, showing that even for the low polynomial order $k = 2$, the DG solver provides accurate solutions for these cases, where detached flow over the blades and blade–wake interactions are present (as discussed below).

Let us now extend the results for $k = 2$ and the normal force (C_N) to 11 revolutions for $\lambda = 1, 2$ and 5 and focus attention on the influence of the upstream blade passage ($0^\circ + 360^\circ i < \theta < 180^\circ + 360^\circ i$, with $i = 0, 1, 2, ..$ an integer denoting the number of rotations) on the downstream blade passage ($180^\circ + 360^\circ i < \theta < 360^\circ + 360^\circ i$). Results are shown in Fig. 6.

First, it can be observed that for all tip speed ratios the forces on the downstream passage are not the same as that on the upstream passage, as might be intuitively expected for a one bladed turbine. Furthermore, the differences between the upstream and downstream passages increase with the tip speed ratio λ.

The force traces depicted in Fig. 6 illustrate the previous discussed limiting cases: for $\lambda = 1 < \lambda_{lim1} \approx 1.6$, interactions are limited to $180^\circ + 360^\circ i < \theta < 270^\circ + 360^\circ i$ (black arrow in Fig. 6 that corresponds to the sketch Fig. 2b.1). For $\lambda_{lim1} < \lambda = 2 < \lambda_{lim2} \approx 4.7$, interactions are limited to $180^\circ + 360^\circ i < \theta < 360^\circ + 360^\circ i$ (red arrow in Fig. 6 and sketch Fig. 2b.2). For $\lambda_{lim2} < \lambda = 5$, interactions are of non-linear type (i.e. cumulative wake effect) showing no clear periodic character (blue arrow in Fig. 6 and sketch Fig. 2b.3).

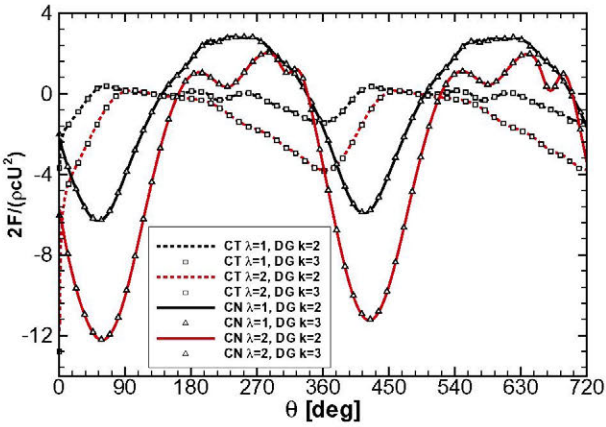

Fig. 5. Tangential and normal force coefficients against azimuth, one bladed turbine for tip speed ratios: $\lambda = 1$ and 2 and polynomial orders: $k = 2$ and 3.

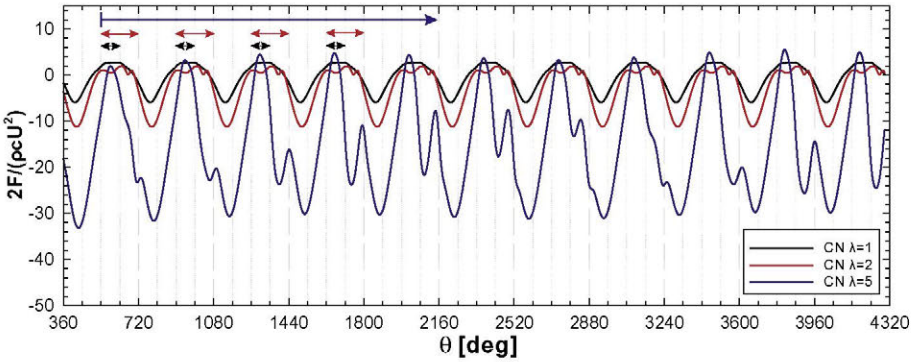

Fig. 6. Normal force coefficient against azimuth, one bladed turbine for $\lambda = 1, 2, 5$. Plot shows 11 revolutions.

We finalise this section illustrating these interactions in Fig. 7. The figure shows velocity contours and streamlines for the three tip speed ratios considered. These snapshots depict the regions where interactions take place. Namely, interactions can be seen in the rear passage for $\lambda = 1$ (low rear quadrant) and $\lambda = 2$ (rear half), whilst interactions of non-linear type are shown for $\lambda = 5$.

3.2.2. One bladed vs three bladed turbine

This section compares one and three bladed turbines for tip speed ratios $\lambda = 1$ and 2. Fig. 8 depicts the force traces for a single blade over 6 revolutions (starting on the second). The figure shows that for the upstream passage ($360° + 360°i < \theta < 540° + 360°i$), the three bladed turbine presents lower forces than observed for the one bladed turbine. These lower forces can be explained by considering the greater streamline deflection for the three bladed turbine due to its higher solidity (effectively higher flow resistance). Deflection of the flow leads to a lower induced *AOA* and U_{eff} which leads to reduced loads. On the downstream passage, the blade of the three bladed turbine sees a more perturbed and slower flow than the one bladed turbine, resulting in lower forces.

Fig. 8a shows that for the three bladed turbine and for $\lambda_{lim1} < \lambda = 1 < \lambda_{lim2}$, blade–wake interactions are limited to $180° + 360°i < \theta < 360° + 360°i$. For the higher tip speed ratio $\lambda_{lim2} < \lambda = 2 < \lambda_{lim3}$, depicted in Fig. 8b, a non-linear behaviour is observed for the three bladed turbine. The latter non-linear effect was observed for $\lambda = 5$ when simulating the one bladed turbine (see Fig. 6). Note that the lower limiting tip speed ratio found for the three bladed turbines is consistent with our analytical estimates.

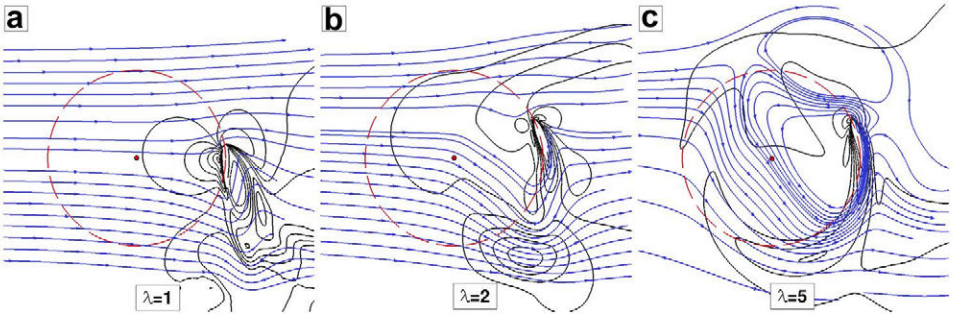

Fig. 7. Velocity magnitude contours and streamlines for one bladed turbine and tip speed ratios: (a) $\lambda = 1$, (b) $\lambda = 2$ and (c) $\lambda = 5$. Red dashed line shows the circular blade path.

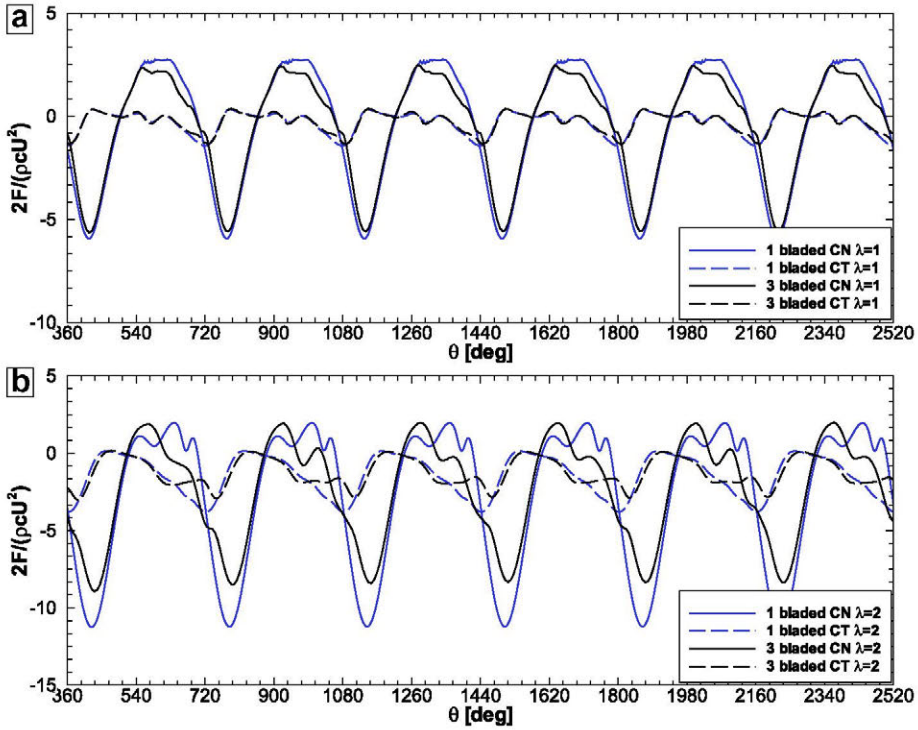

Fig. 8. Tangential and normal force coefficients against azimuth, one and three bladed turbines: (a) $\lambda = 1$ and (b) $\lambda = 2$. Forces shown are for a single blade.

Let us finally note that, to the authors' knowledge, the effect of blade–wake interactions on three bladed turbines has not been fully assessed in the past. A possible explanation is that, generally, integrated or averaged forces for the three blades are studied. The integration or averaging process can mask blade–wake interaction effects on individual blades. In the present work, the force traces have been studied for a single blade even when considering three bladed turbine configurations, which has enabled the exploration of these interactions.

Finally, this section has shown that the analytical bounds agree well with the fully resolved simulations.

4. Conclusions

Analytical estimates to bound blade–wake interactions have been derived, and may help to understand the fluid–structure interactions involved in cross-flow turbines. A summary of the analytical bounds for one and three bladed turbines can be found in Table 1 which includes limiting tip speed ratios, the type of interactions together with the azimuth angles where the effect is seen when analysing the blade forces.

These bounds, that have been numerically validated using a high order Discontinuous Galerkin solver, provide useful information that may be used to correct simple design codes (e.g. based on Blade Element Momentum techniques) that are not naturally able to cope with complex flow interaction phenomena.

Acknowledgements

EF would like to acknowledge the financial support of the John Fell OUP fund (2008-2012) and the European Commission (ANADE project under grant contract PITN-GA-289428). RW would like to thank RCUK for the financial support.

Appendix A. Reynolds number effects

In this appendix we include simulations using the high order DG solver for a one bladed turbine and a range of Reynolds numbers. The tip speed ratio is fixed to $\lambda = 1$ (using $U = 0.2$ m/s and

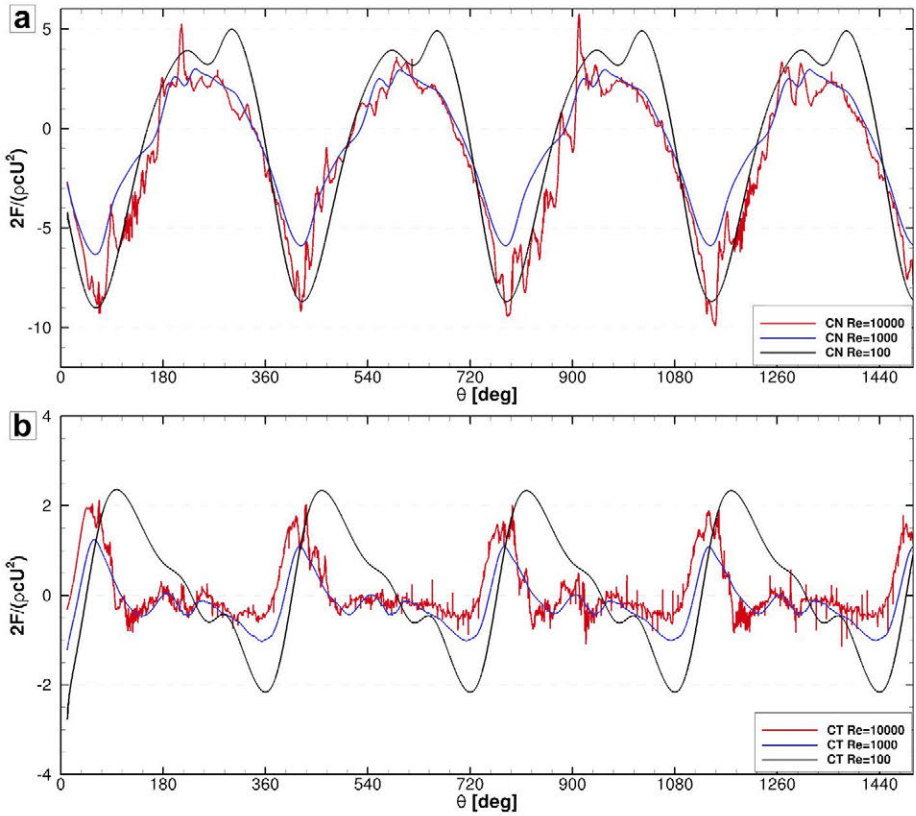

Fig. 9. Force coefficients against azimuth for one bladed turbines for $\lambda = 1$ and varying Reynolds numbers Re = 100, 1000, 10.000: (a) normal and (b) tangential force component. Forces shown are for a single blade.

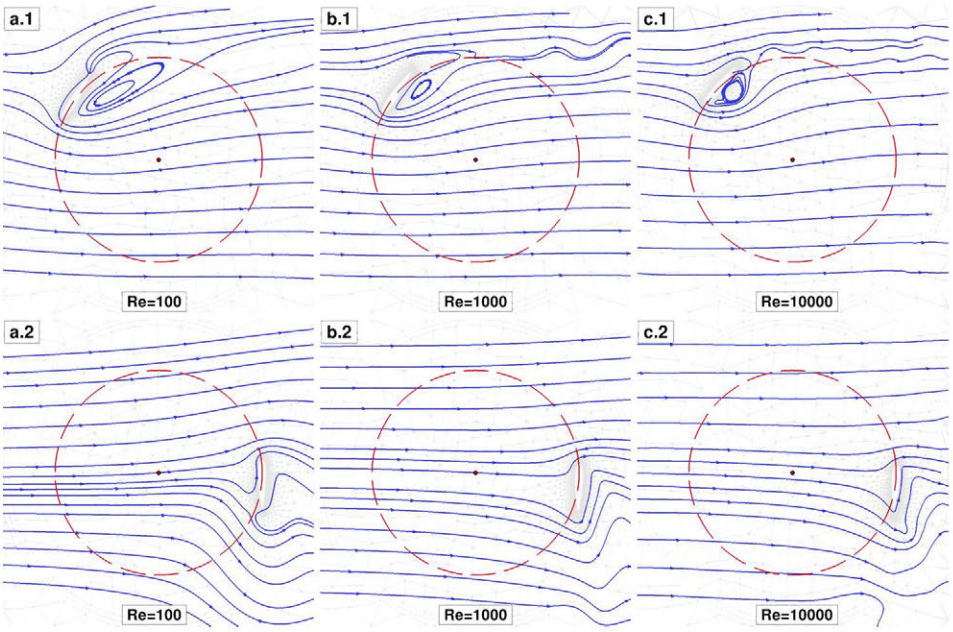

Fig. 10. Velocity streamlines for one bladed turbine, tip speed ratio $\lambda = 1$ and Reynolds number: (a) $Re = 100$, (b) $Re = 1000$ and (c) $\mathrm{Re} = 10.000$. Red dashed line shows the circular blade path.

$\omega = 0.1$ rad/s). Fig. 9 shows the force traces for three Reynolds numbers: $\mathrm{Re} = 100,\ 1000,\ 10.000$. It can be seen that the normal force components, Fig. 9a, do not show significant differences when varying the Reynolds number. More importantly, the blade–wake interactions are limited to the rear blade passage for all Reynolds at the given tip speed ratio. The tangential forces depicted in Fig. 9b show a non-negligible influence when varying the Reynolds number, which is caused by variations of viscous effects on drag. Indeed, the tangential force component is more influenced by drag that the normal component in cross-flow turbines.

For completeness, we show in Fig. 10 flow field snapshots for the three Reynolds numbers. It can be seen in Fig. 10a.1, b.1 and c.1 that the upstream wake generation phenomena are similar although the wake is wider and larger for $Re = 100$. Finally, inspection of the blade rear passage (Fig. 10a.2, b.2 and c.2) show that the blade–wake interactions are of similar type for all Reynolds.

References

[1] I. Afgan, J. McNaughton, S. Rolfo, D.D. Apsley, T. Stallard, P. Stansby, Turbulent flow and loading on a tidal stream turbine by LES and RANS, Int. J. Heat Fluid Flow 43 (0) (2013) 96–108.
[2] Y. Bazilevs, A. Korobenko, X. Deng, J. Yan, M. Kinzel, J.O. Dabiri. Fluid structure interaction modeling of vertical axis wind turbines. J. Appl. Mech., 81.
[3] C.A. Consul, R.H. Willden, S.C. McIntosh, Blockage effects on the hydrodynamic performance of a marine cross-flow turbine, Philos. Trans. Ser. A, Math., Phys., Eng. Sci. 371 (2013).
[4] R.F. Day, H.A. Stone, Lubrication analysis and boundary integral simulations of a viscous micropump, J. Fluid Mech. 416 (2000) 197–216. 8.
[5] D. Decourtye, M. Sen, M. Gad-el Hak, Analysis of viscous micropumps and microturbines, Int. J. Comput. Fluid Dyn. 10 (1) (1998) 13–25.
[6] T.L. Doligalski, C.R. Smith, J.D.A. Walker, Vortex interactions with walls, Annu. Rev. Fluid Mech. 26 (1) (1994) 573–616.
[7] S. Draper. Tidal Stream Energy Extraction in Coastal Basins. PhD Thesis, University of Oxford, 2011.
[8] S. Eriksson, H. Bernhoff, M. Leijon, Evaluation of different turbine concepts for wind power, Renew. Sustain. Energy Rev. 12 (5) (2008) 1419–1434.
[9] E. Fernandez-Rodriguez, T.J. Stallard, P.K. Stansby, Experimental study of extreme thrust on a tidal stream rotor due to turbulent flow and with opposing waves, J. Fluids Struct. 51 (0) (2014) 354–361.

[10] E. Ferrer, A High Order Discontinuous Galerkin – Fourier Incompressible 3D Navier–Stokes Solver with Rotating Sliding Meshes for Simulating Cross-flow Turbines. PhD Thesis, University of Oxford, 2012.
[11] E. Ferrer, D. Moxey, R.H.J. Willden, S. Sherwin, Stability of projection methods for incompressible flows using high order pressure–velocity pairs of same degree: continuous and Discontinuous Galerkin formulations, Commun. Comput. Phys. 16 (3) (2014) 817–840.
[12] E. Ferrer, R.H.J. Willden, A high order Discontinuous Galerkin Finite Element solver for the incompressible Navier–Stokes equations, Comput. Fluids 46 (1) (2011) 224–230.
[13] E. Ferrer, R.H.J. Willden, A high order Discontinuous Galerkin – Fourier incompressible 3D Navier–Stokes solver with rotating sliding meshes, J. Comput. Phys. 231 (21) (2012) 7037–7056.
[14] N. Hill, R. Dominy, G. Ingram, J. Dominy, Darrieus turbines: the physics of self-starting, Proc. Inst. Mech. Eng. Part A – J. Power Energy 223 (2009) 21–29.
[15] G.T. Houlsby, S. Draper, M.L.G Oldefield. Application of Linear Momentum Actuator Disc Theory to Open Channel Flows. Technical Report, Oxford University Engineering Library Report, 2008.
[16] R. Howell, N. Qin, J. Edwards, N. Durrani, Wind tunnel and numerical study of a small vertical axis wind turbine, Wind Eng. 35 (2010) 412–422.
[17] M.C. Hsu, I. Akkerman, Y. Bazilevs, High-performance computing of wind turbine aerodynamics using isogeometric analysis, Comput. Fluids 49 (1) (2011) 93–100.
[18] M. Islam, D.S.K. Ting, A. Fartaj, Aerodynamic models for Darrieus-type straight-bladed vertical axis wind turbines, Renew. Sustain. Energy Rev. 12 (4) (2008) 087–1109.
[19] C. Li, S. Zhu, Y. Xu, Y. Xiao, 2.5d Large Eddy Simulation of vertical axis wind turbine in consideration of high angle of attack flow, Renew. Energy 51 (0) (2013) 317–330.
[20] K. McLaren, S. Tullis, S. Ziada, Computational fluid dynamics simulation of the aerodynamics of a high solidity, small-scale vertical axis wind turbine, Wind Energy 3 (2011) 349–361.
[21] K. McLaren, S. Tullis, S. Ziada, Measurement of high solidity vertical axis wind turbine aerodynamic loads under high vibration response conditions, J. Fluids Struct. 32 (0) (2012) 12–26.
[22] J. McNaughton, F. Billard, A. Revell, Turbulence modelling of low Reynolds number flow effects around a vertical axis turbine at a range of tip-speed ratios, J. Fluids Struct. 47 (0) (2014) 124–138.
[23] G. Muller, M.F. Jentsch, E. Stoddart, Vertical axis resistance type wind turbines for use in buildings, Renew. Energy 34 (5) (2009) 1407–1412.
[24] B.G. Newman, Actuator-disc theory for vertical-axis wind turbines, J. Wind Eng. Ind. Aerodyn. 15 (1-3) (1983) 347–355.
[25] N. Qin, R. Howell, N. Durrani, K. Hamada, T. Smith, Unsteady flow simulation and dynamic stall behaviour of vertical axis wind turbine blades, Wind Eng. 35 (4) (2011) 511–527.
[26] D. Rockwell, Vortex–body interactions, Annu. Rev. Fluid Mech. 30 (1) (1998) 199–229.
[27] A. Rossetti, G. Pavesi, Comparison of different numerical approaches to the study of the H-Darrieus turbines start-up, Renew. Energy 50 (2013) 7–19.
[28] F. Scheurich, T.M. Fletcher, R.E. Brown, Simulating the aerodynamic performance and wake dynamics of a vertical-axis wind turbine, Wind Energy 14 (2) (2011) 159–177.
[29] J. Seydel, A. Aliseda, Wind turbine performance in shear flow and in the wake of another turbine through high fidelity numerical simulations with moving mesh technique. Wind Energy, 16(1).
[30] L. Shi, V.A. Riziotis, S.G. Voutsinas, J. Wang, A consistent vortex model for the aerodynamic analysis of vertical axis wind turbines, J. Wind Eng. Ind. Aerodyn. 135 (0) (2014) 57–69.
[31] J.H. Strickland. Darrieus Turbine: A Performance Prediction Model Using Multiple Streamtubes. Technical Report No. SAND-75-0431, Sandia Labs, 1975.
[32] R.J. Templin. Aerodynamic Performance Theory for the NRC Vertical-axis Wind Turbine. NASA STI/Recon Technical Report N, 76, 1974.
[33] W. Tjiu, T. Marnoto, S. Mat, M.H. Ruslan, K. Sopian, Darrieus vertical axis wind turbine for power generation I: assessment of Darrieus VAWT configurations, Renew. Energy 75 (0) (2015) 50–67.
[34] J.I. Whelan, J.M.R. Graham, J. Peiro, A free-surface and blockage correction for tidal turbines, J. Fluid Mech. 624 (2009) 281–291. 4.
[35] R.E. Wilson, P.B.S. Lissaman. Applied Aerodynamics of Wind Power Machines. NASA STI/Recon Technical Report, 75:22669, July 1974.